Machine-learning-enhanced phase-based multi-tone continuous-wave lidar

M. Mert Bayer, Berken Utku Demirel, Ataberk Atalar, Xun Li, Haoyu Xie, et al.

M. Mert Bayer, Berken Utku Demirel, Ataberk Atalar, Xun Li, Haoyu Xie, Ozdal Boyraz, "Machine-learning-enhanced phase-based multi-tone continuous-wave lidar," Proc. SPIE 12428, Photonic Instrumentation Engineering X, 124280I (8 March 2023); doi: 10.1117/12.2650368

SPIE.

Event: SPIE OPTO, 2023, San Francisco, California, United States

Machine Learning Enhanced Phase-Based Multi-Tone Continuous-Wave Lidar

M. Mert Bayer[a], Berken Utku Demirel[a], Ataberk Atalar [a], Xun Li [a], Haoyu Xie [a], Ozdal Boyraz*[a]
[a]Electrical Engineering and Computer Science Department, University of California, Irvine, CA 92697 USA

ABSTRACT

Lidar technologies have been investigated and commercialized for various applications such as autonomous driving and aerial vehicles. The pulsed time of flight and frequency-modulated continuous-wave lidars are the two common lidar technologies that dominate. As an alternative to the available lidars, we developed the phase-based multi-tone continuous-wave (PB-MTCW) technology that can perform single-shot simultaneous ranging and velocimetry measurements with a high resolution at distances far beyond the coherence length of a CW laser, without employing any form of sweeping. The proposed technique utilizes relative phase accumulations at phase-locked RF sidebands to identify the range of the target after a heterodyne detection of the beating of the echo signal with an unmodulated CW optical local oscillator (LO). Up-to-date, we demonstrated that the PB-MTCW lidar could perform ranging ×500 beyond the coherence length of the laser with <1cm precision. Here, we implement machine learning (ML) algorithms to the PB-MTCW architecture to improve the ranging resolution, as well as to provide a solution to multi-target reflections using tone-amplitude variations. We used four different training schemes by utilizing the acquired RF tones and phases from simulation results, experimental results, and their combinations in a convolutional neural network model. We demonstrate that the ML algorithm yields an average mean square error of ~0.3mm compared to the actual target distance, hence enhancing the ranging resolution of PB-MTCW lidar. It is also shown that the ML algorithm can distinguish multiple targets in the same line of sight with a 98%±0.7% success rate depending on the targets' reflectance and distances.

Keywords: Lidar, machine learning, optical reflection measurement

1. INTRODUCTION

Sensor fusion has produced an enormous amount of data over time, which is too much for conventional computational techniques to process. Artificial intelligence (AI) and machine learning (ML) have emerged as natural entryways to reduce data clogs and effectively use details that are disregarded by conventional techniques[1–3]. While ML algorithms can now recognize, classify, and route data without making extensive observations, AI algorithms make judgments about the nature of data and take action without requiring human involvement[4,5]. Despite the significant advancements in AI and ML in other fields, forestry and autonomous vehicle applications rarely use optical lidar-based sensing technologies [6–10].

In particular, light detection and ranging (lidar) techniques are researched and used in practical applications such as forestry, oceanography, autonomous driving, and precision measurements[11–14]. To do so, various lidar methods have been developed including coherent lidars that use amplitude, phase, or frequency-modulated continuous-wave (CW) light[15–17] and pulsed lidars that operate by direct light detection of laser pulse propagation for time-of-flight measurements[18–21]. The signal-to-noise ratio (SNR) of the detection is improved with the coherent lidars' because the detection scheme is constrained by the shot noise[22]. However, CW lidars rely on a phase or frequency sweep of the light, which restricts their ability to operate in a single shot for swiftly moving platforms like CubeSats or airborne lidars [23]. In addition, despite the fact that the CW configuration improves range resolution and offers simultaneous velocimetry capability via the Doppler effect [24–28], the maximum detection range, or the laser's coherence length, is limited by the laser phase noise.

We previously introduced and demonstrated the phase-based multi-tone continuous-wave (PB-MTCW) lidar, which can perform ranging well beyond the coherence length of a CW laser, to address the aforementioned constraints on coherent lidars [29]. In this method, the output of a CW laser is divided, one arm is amplitude modulated with a number of phase-locked radio frequencies (RF), and the other branch is left unmodulated to serve as a local oscillator (LO) for shot noise-limited heterodyne detection. Each RF tone accumulates a different phase in the echo signal depending on the tone frequency and the target distance. Since the tones are all contained within the same optical carrier, the common phase-noise components can be eliminated by RF mixing the different detected tones. As a result, position triangulation algorithms can use the phase-noise-free terms by using a variety of tone frequencies and tone phases [30,31]. Additionally,

Photonic Instrumentation Engineering X, edited by Lynda E. Busse, Yakov Soskind, Proc. of SPIE
Vol. 12428, 124280I · © 2023 SPIE · 0277-786X · doi: 10.1117/12.2650368

the PB-MTCW technique can make use of the Doppler frequency shifts to compute the target velocity in addition to the ranging, just like the other coherent lidars. We have previously shown that the PB-MTCW technique performs with a precision of 1cm over a range of 500 more than the coherence length of CW lasers. The localization of targets for autonomous vehicles using the same method is also possible.

One of the three measurable quantities amplitude, frequency, or phase is the main focus of all developments in the lidar field [16,32]. Here, we postulate that it is possible to increase measurement accuracy and offer a solution to multi-path interference and multi-surface reflections [33,34] by training an ML algorithm using all the characteristics of stable RF tones, including the phase, frequency, and amplitude information. When a complicated target geometry is positioned in front of the beam, this theory is correct. In this work, we demonstrate how ML algorithms and pattern recognition techniques can be used to improve the PB-MTCW technique. We create ML algorithms in particular that make use of all three measurable parameters to recognize complex target structures. The RF tones will experience amplitude variations as a result of light interference when the lidar aperture simultaneously receives two multi-tone modulated echo signals from various surfaces in the same line of sight. Based on the target distances and tone frequencies, these amplitude variations vary. The pre-trained ML algorithm can be used to estimate the existence of multiple targets as well as the distances of both targets by making use of the relative amplitude variations between the individual tones. We use simulation and experimental data to show the technique's effectiveness. We demonstrate that we can locate the positions of multiple targets with a 5 cm error and estimate multi-path interference with 98%±0.7% accuracy. Similar to this, the ML algorithm can accurately verify a single reflection with >97%. Additionally, we show that the ML algorithm produces an average mean square error of 0.3mm, improving the ranging accuracy of the PB-MTCW lidar. This method has the potential to help precise navigation and localization applications [35] and to address multi-path interference, one of the main problems with current lidar techniques.

2. PHASE-BASED MULTI-TONE CONTINUOUS-WAVE LIDAR

2.1 Concept

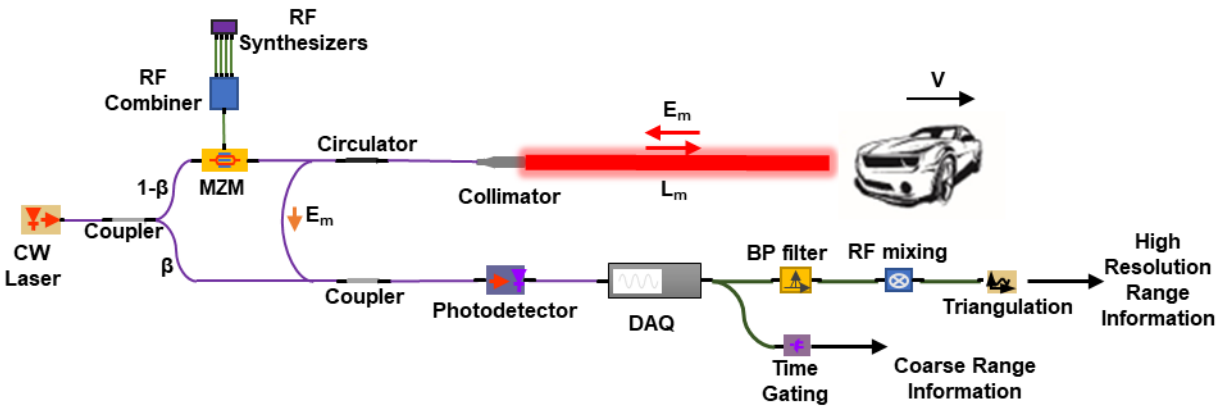

Figure 1. Operating theory of the Phase-Based Multi-Tone Continuous Wave lidar.

A continuous wave laser is modulated using a Mach Zehnder modulator in the previously demonstrated Phase-Based Multi-Tone Continuous Wave lidar (PB-MTCW) method [29]. Each tone has a frequency of f_i. After light propagation, the accumulated phases of these tones are encoded in the echo signal. Based on the target distance, L_m, and light speed, c, each modulation tone will accumulate a phase as $\phi_i^{range} = \left(2L_m\omega_i\right)/c$, where $\omega_i = 2\pi f_i$. An unmodulated local oscillator (LO) is then used to further obstruct the received signal in order to collect the beat notes and achieve shot-noise limited detection. Each tone is filtered with low bandwidth bandpass filters using the a priori knowledge of the chosen tone frequencies. The phase-noise-free intermediate frequencies (IF) are produced by further RF combining the individual tones. The target position can be triangulated using the phase and frequency information of the resulting IFs because there are multiple IF terms with specific phases, as shown in Figure 1.

2.2 Theoretical Model

According to theory, the CW laser's electric field (E-field) is defined as $E_{laser} = A_0 \exp(j\omega_0 t + j\phi_0)$, where $A_0 = \sqrt{P_{out}}$ is the amplitude ω_0 is the optical carrier frequency and ϕ_0 is the source laser's initial phase. A coupler with a β/(1-β) power splitting ratio is then used to split the laser into two. By also taking into account fiber attenuation (α_f) and laser phase noise ($\phi_n(t-\tau_{LO})$), where τ_{LO} is the propagation time in the local oscillator branch, the unmodulated local oscillator is formulated as in Eq. (1).

$$E_{LO} = A_0 \alpha_f \sqrt{\beta} \exp(j\omega_0 t + j\phi_0 + j\phi_n(t-\tau_{LO})) \tag{1}$$

The E-field of the echo signal is presented in Eq.(2) after defining the linear attenuation coefficient (α_m) related to the potential scattering, collection, and/or back coupling losses.

$$\begin{aligned} E_m = {} & \frac{A_0}{2\sqrt{2}} \alpha_m \alpha_f \sqrt{1-\beta} \exp\left[j\omega_0 t + j\phi_0 + j\omega_0 \frac{2L_m}{c} + j\phi_n(t-\tau) \right] \\ & - \frac{mA_0}{4\sqrt{2}} \alpha_m \alpha_f \sqrt{1-\beta} \sum_{i=1}^{N} \left(\begin{array}{l} \exp\left[j(\omega_0+\omega_i)t + j\phi_0 + j\phi_i^{RF} + j(\omega_0+\omega_i)\frac{2L_m}{c} + j\phi_n(t-\tau) \right] \\ + \exp\left[j(\omega_0-\omega_i)t + j\phi_0 - j\phi_i^{RF} + j(\omega_0-\omega_i)\frac{2L_m}{c} - j\phi_n(t-\tau) \right] \end{array} \right) \end{aligned} \tag{2}$$

$\phi_n(t-\tau)$ is the laser phase noise associated with τ, which is the time when the laser beam first exits the MZM, and $\tau = 2L_m / c$ is the propagation time in this instance. Every modulation frequency will carry the same noise term because the defined phase noise term is related to the carrier. Through the use of a Y-coupler, the E_m and E_{LO} are combined to produce $I_{pd} = R(E_m + E_{LO}) \cdot (E_m + E_{LO})^*$ as the photocurrent. Eq. (3) illustrates the final I_{pd} following the local oscillator's interference with the echo signal from a stationary target, where the laser phase noise difference between E_m and E_{LO} is represented as $\Phi(t,\tau,\tau_{LO}) = \phi_n(t-\tau_{LO}) - \phi_n(t-\tau)$ [33].

$$\begin{aligned} I_{pd} = {} & RA_0^2 \alpha_f^2 \beta + \frac{3RA_0^2 \alpha_m^2 \alpha_f^2 (1-\beta)}{16} + \frac{RA_0^2 \alpha_m \alpha_f^2 \sqrt{\beta}\sqrt{1-\beta}}{\sqrt{2}} \cos\left(\omega_0 \frac{2L_m}{c} + \Phi(t,\tau,\tau_{LO}) \right) \\ & - \frac{RmA_0^2 \alpha_m \alpha_f^2 \sqrt{\beta}\sqrt{1-\beta}}{2\sqrt{2}} \left[\begin{array}{l} \sum_{i=1}^{N} \cos\left(\omega_i t + (\omega_0+\omega_i)\frac{2L_m}{c} + \phi_i^{RF} + \Phi(t,\tau,\tau_{LO}) \right) \\ + \sum_{i=1}^{N} \cos\left(\omega_i t - (\omega_0-\omega_i)\frac{2L_m}{c} - \phi_i^{RF} - \Phi(t,\tau,\tau_{LO}) \right) \end{array} \right] \\ & + \frac{RmA_0^2 \alpha_m^2 \alpha_f^2 (1-\beta)}{8} \left[\sum_{i=1}^{N} \cos\left(\omega_i t + \omega_i \frac{2L_m}{c} + \phi_i^{RF} \right) + \sum_{i=1}^{N} \cos\left(\omega_i t + \omega_i \frac{2L_m}{c} - \phi_i^{RF} \right) \right] \\ & + \frac{Rm^2 A_0^2 \alpha_m^2 \alpha_f^2 (1-\beta)}{8} \sum_{i=1}^{N} \cos\left(2\omega_i t + \omega_i \frac{4L_m}{c} \right) \end{aligned} \tag{3}$$

By using narrow bandwidth bandpass filters centered at each frequency, it is possible to separate the individual tones using the resulting photocurrent. The common phase-noise terms brought on by the optical carrier can then be eliminated by RF mixing the filtered tones. The IF is expressed as $A_i A_j \cos(\Delta\omega_{i,j} t \pm \Delta\phi_{i,j})$ after the RF mixing of two of these distinct tones at ω_i and ω_j ($i \neq j$), where $\Delta\phi_{i,j}$, and $\Delta\omega_{i,j}$ are the phase and frequency differences of the i^{th} and j^{th} tones, respectively.

Further definition of the target's range is $L_m = (2\pi n + \Delta\phi_{i,j}) c / \Delta\omega_{i,j}$, where n is an integer. Periodic range estimation will be produced by the modulo-2π behavior of the phase, which is cyclic. Redundancy through the use of multiple agents, which is provided by the abundance of modulation tones, is required to achieve accurate range information. For a specific n, the L_m solution for each $\Delta\omega_{i,j}$ should converge to a single value. We created a triangulation algorithm to find the common solution, which generates all possible solutions for each IF by sweeping the integer values of n. Then, by obtaining the common solution for all IFs, we estimate the target range [29,30].

2.3 Experimental Setup

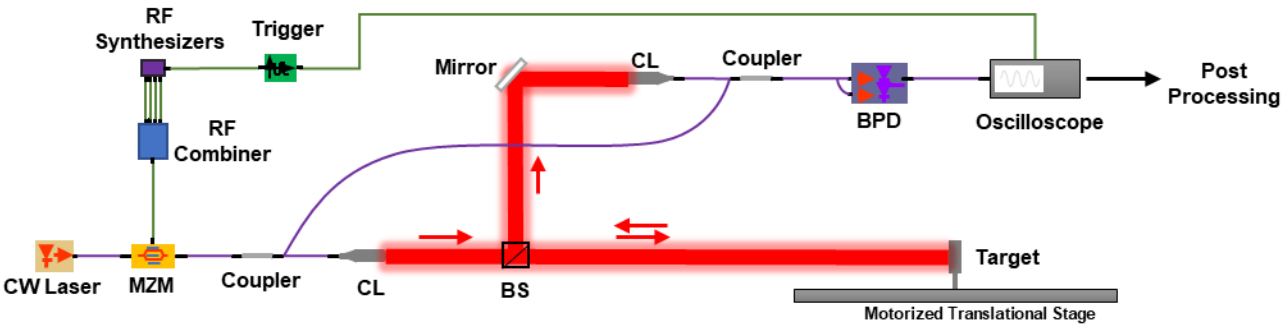

Figure 2. The experimental setup for PB-MTCW. Collimator (CL), beamsplitter (BS), Mach-Zehnder modulator (MZM), and balanced photodetector (BPD).

A static target's position is determined using the experimental setup depicted in Figure 2. An MZM (iXblue - NIR-MX-LN series), which is optimized for 1064nm and has a 30dB extinction ratio, with four applied modulation frequencies at 300, 500, 890, and 1350MHz, is used to modulate a CW laser with a linewidth of about 100kHz at 1064nm (RPMC Lasers - R1064SB0300PA). To avoid second harmonic mixing or frequency overlap, these modulation frequencies were carefully chosen. The oscilloscope and a 10MHz common clock are used to trigger phase-locked RF synthesizers (Windfreak Technologies - SynthHD (v2)) that produce the tones. On a motorized translational stage, the target reflector is put, and over the course of several trials, the target is moved on the stage in 2 cm steps. Utilizing a (CL), the modulated light is sent into free space and coupled back to another collimator for collection. Through an optical Y-coupler, the collected signal interferes with the LO. The two halves of the final light signal are fed to a high-speed balanced photodetector (PDB482C-AC), which has a bandwidth of 2.5GHz and a noise equivalent power of 12pW/Hz$^{1/2}$. To calibrate the lidar, the initial tone phases are measured at the MZM's output facet. Prior to taking measurements of the target, the post-processing algorithm uses the measurement made at the calibration mirror as the lidar system's zero point. With a time window of 100μs and a sampling rate of 10 GS/s, a digital storage oscilloscope is used for acquisition, producing a time resolution of 0.1 nm. Range resolution, or δL, is determined by the minimum phase of the ith tone, $d\phi_i$, as $\delta L = c \times d\phi_i / \omega_i = c \times dt$, which is related to the time resolution. By taking into account a noise-free case, where $d\phi_i = \omega_i \times dt$, and consequently $\delta L = c \times dt$, where dt is the time resolution, the minimum theoretical resolution can be formalized. Without any additional post-processing, the theoretical minimum resolution for the experiment is about 3 cm. After separating the phase and frequency of the IF tones, the target ranges are first calculated using the triangulation algorithm. The ML algorithms are then given the extracted tone data to estimate the target range. The outcomes of the ML algorithms are then contrasted with the data from the PB-MTCW lidar, actual target ranges, and target distances.

3. MACHINE LEARNING ALGORITHM

In order to highlight the relationships between the PB-MTCW and distance, we formulate the distance estimation problem based on a fundamental regression model, mapping a time-series input to a value. The input and output pairs of the ML model are defined as follows for the proposed basic regression model. Each sample is labeled during training with the true distance measurements discovered by the triangulation algorithm. The phase and frequency of the IF tones, which are extracted as previously mentioned, serve as the model's input.

We write the extracted phase and frequency values at a point as (ϕ, ω), where ϕ is the vector made up of the phase values and is the number of tones that were used. The triangulation algorithm's output, denoted as L, represents the true distance value. When using the input and model parameters, the designed ML model is parametrized by Φ, and the overall regression is given in Eq. (4), where $\hat{L}$ is the target's estimated distance value. To reduce the error between the model's output, $\hat{L}$, and the actual distance to the target, L, we used the L1 loss, also known as Mean Absolute Error, when training the model. Using the trained model f with parameters Φ, as shown in Eq. (4), the task during the test is to estimate the true distance L given the extracted phase and tone pairs (ϕ, ω) of a sample. The input pair is changed to the magnitude with frequency tones rather than the phase to differentiate the number of targets. And L1 is replaced by the cross-entropy loss.

Only the phase and frequency tone pairs are used as input in the specifically designed regression model; other raw signal or system-related features, such as the magnitude or information on the reflection coefficient, are not used to calculate the target's distance.

$$\hat{L} = f(\phi, \omega, \Phi) \tag{4}$$

The regression model is made up of three main layers. The input layer, which has twice as many units as the second layer and contains the extracted phase values, is fed into the machine learning model first. Two hidden layers with 256 and 128 units each make up the second layer, which is used to extract features from the input pair. The output layer, which is the final layer of the model, provides the estimated distance. Glorot initialization of the weights was used to train the network [36]. For each dense layer, L2-regularization with 0.001 is used to avoid overfitting. With the default values of ß1=0.9 and ß2=0.999 and a mini-batch size of 120, we used the Adam optimizer [37]. When the validation mean squared error stopped decreasing for 75 consecutive epochs, the learning rate was reduced from its initial value of 0.002 by a factor of 10. With a maximum of 900 epochs, training continues until 100 consecutive epochs without performance improvements. The model with the lowest loss on the validation data is deemed the best. The network architecture and the optimization algorithm hyperparameters were typically selected through manual tuning. To find the most effective model for the estimation, we essentially searched over the quantity of hidden layers and units.

Without altering or changing the model's hyperparameters, the ML model is evaluated using all of the recorded data. The model only modifies the input when it attempts to distinguish between the previously mentioned single target and two targets. We used leave distance out cross-validation, which is similar to leave one out cross-validation (LOOCV[38]), to assess the trained model's generalizability. The employed validation technique guarantees that the trained ML model is capable of generalizing target distance values that the model has not encountered during training. For instance, only the phase values corresponding to distances between 10 and 11 cm are observed by the model during training. Additionally, the phase values at a distance of 10.5 cm are fed into the model for the inference (test). In this way, we have followed a principled approach to assess the effectiveness of the suggested method.

In the section that follows, we present the results of a single, one-off experiment in which the training and validation splits were determined at random. In order to implement early stopping based on the validation loss and prevent overfitting, 10% of training records were used for validation. As part of the partitioning process for the validation and training data, various percentages are also used. However, 10% of the data for validation and 90% for training have been shown to perform the best.

4. RESULTS

To see if the suggested method works well for estimating the target distance values, we conducted a wide range of experiments. In terms of noise level and target distances, these tests aimed to assess the performance measures and the model's capabilities. The performance of the target distance estimation is measured using the metrics Mean Absolute Error (MAE) and Root Mean Squared Error (RMSE). The estimation values, $\hat{L}$, and actual target distance, L, which are discovered through triangulation, are used to calculate the metrics. Eq (5) illustrates how MAE is calculated.

$$MAE = \frac{\sum_{i=1}^{n} |L_i - \hat{L_i}|}{n} \tag{5}$$

We adjusted the target distance range, the number of tones with various tone values, and the noise factor in order to evaluate the model's performance thoroughly. In total, we carried out the three main experiments listed as follows. 1) Noiseless single target distance estimation. 2) Noiseless double target differentiation with distance estimation. 3) Single target lab environment distance estimation.

$Tones_1$ = [20MHz, 500MHz, 700MHz, 850MHz, 950MHz], $Tones_2$ = [500 MHz, 700 MHz, 850 MHz, 950MHz], and $Tones_3$ = [700MHz, 850 MHz, 950 MHz, 1050 MHz] are the three pairs we selected for the tone frequency variations. We thoroughly assessed the machine learning model's performance on the task by selecting various numbers of tones with values. In addition, we have replaced the target distance values L1 and L2 with the target reflection coefficients. The outcomes of our experiments are compiled in the following three tables.

Table 1. The first case of the evaluation scheme, the evaluation of the estimation errors of the trained ML model for a single target at three distinct tones with three separated distances.

Tones / L_1 (m)	**0.1-3**	**0.1-5**	**0.1-10**
Tones$_1$	0.0020 ± 0.001 dm	0.0023 ± 0.001 dm	0.0025 ± 0.001 dm
Tones$_2$	0.0003 ± 0.0002 dm	0.00032 ± 0.0001 dm	0.00035 ± 0.002 dm
Tones$_3$	0.0001 ± 0.0001 dm	0.00002 ± 0.001 dm	0.00001 ± 0.001 dm

The ML regression model's average estimation error and standard deviations for training with the previously mentioned three different tones are displayed in Table 1. The data in Table 1 show that the proposed ML model with feature extraction can accurately estimate the target distance. The model performs best when it is trained and assessed using Tones3, with an average mean error of 0.0002 cm. The importance of tone selection is demonstrated by the model's performance declining by about 10 times when it is trained with first tone combinations.

Table 2. The second case of the evaluation scheme, the evaluation of the estimation errors of the trained ML model at three distinct tones and three separated distances for the first target of the double target.

Tones / L_1 (m)	**0.1-3**	**0.1-5**	**0.1-10**
Tones$_1$	0.0010 ± 0.005 dm	0.0023 ± 0.001 dm	0.0025 ± 0.001 dm
Tones$_2$	0.0002 ± 0.0001 dm	0.00021 ± 0.0001 dm	0.00021 ± 0.0003 dm
Tones$_3$	0.00005 ± 0.00001 dm	0.00006 ± 0.00001 dm	0.00008 ± 0.0001 dm

Table 3. The second case of the evaluation scheme, evaluation of the estimation errors of the trained ML model at three distinct tones and three separated distances for the second target of the double target.

Tones / L2 (m)	**3.1-5**	**3.1-7**	**3.1-10**
Tones$_1$	0.0017 ± 0.003 dm	0.0031 ± 0.005 dm	0.0033 ± 0.005 dm
Tones$_2$	0.000055 ± 0.0003 dm	0.00066 ± 0.0002 dm	0.00072 ± 0.002 dm
Tones$_3$	0.00053 ± 0.0004 dm	0.00062 ± 0.0001 dm	0.00067 ± 0.0003 dm

Tables 2 and 3 display the model's performance in the scenario with two targets. Therefore, we started by analyzing how well the model performed when we varied the number of targets. If there are two targets and the model only predicts one of them, we predict the distance to the first target and report the error for the second target. In other words, while the true distance values remain unchanged, the prediction distance for the second target, $\hat{L}_2$, is set to zero. Tables 1, 2, and 3 show that as a result, the trained ML models' estimation performance for the double target is lower than it was for the single target.

The accuracy of the classifier is %98±0.7 when we evaluated the trained model in terms of the classification performance of the number of targets. We changed the first and second target distances from 0.1-3 meters to 3.1–10 meters, respectively, while evaluating the model. However, the performance comparison of the Tones remains the same. In other words, it is clear from our analysis of the effectiveness of the various *Tones* that *Tones*$_1$ performs the worst in terms of estimating target distance. This consistency across various experimental configurations demonstrates that the extracted phase and magnitude values from the pre-processing have a significant impact on the ML model's performance.

The trained model is then assessed using scheme 3, which is the single target lab environment distance estimation. We had to use a single *Tone* vector with three frequencies, 500 MHz, 700 MHz, and 950 MHz during training and testing, which was a minor difference between the experiment and the other two simulations. The final scheme's overall estimation error is 0.013 ±0.01 dm. The third experimental setup's main flaw is that it needs a lot of data to train the ML model because machine learning is a data-hungry method of system modeling. This flaw prevents the model's performance from being thoroughly experimented with. As a result, we think that fresh approaches to training ML models for similar experimental setups should be suggested.

5. CONCLUSION

This paper introduces a machine-learning-assisted MTCW lidar system that performs target localization using phase information that has been extracted from various tones. We have gathered real data using simulations to test our suggested methodology, and we have used principled cross-validation to test the machine learning model. Our findings demonstrate that the suggested method accurately predicts the distance in three training schemes with a total MSE error of 0.3 mm.

6. ACKNOWLEDGEMENTS

This work was supported by the Office of Naval Research under grant number # N00014-18-1-2845.

7. REFERENCES

[1] Al-Jarrah, O. Y., Yoo, P. D., Muhaidat, S., Karagiannidis, G. K. and Taha, K., "Efficient Machine Learning for Big Data: A Review," Big Data Research **2**(3), 87–93 (2015).

[2] Moorthy, U. and Gandhi, U., "A Survey of Big Data Analytics Using Machine Learning Algorithms Source Title: HCI Challenges and Privacy Preservation in Big Data Security," 99–123 (2019).

[3] Zhou, L., Pan, S., Wang, J. and Vasilakos, A. V., "Machine learning on big data: Opportunities and challenges," Neurocomputing **237**, 350–361 (2017).

[4] Bkassiny, M., Jayaweera, S., Li, Y. and Avery, K., "Wideband Spectrum Sensing and Non-Parametric Signal Classification for Autonomous Self-Learning Cognitive Radios," IEEE Transactions on Wireless Communications **11**, 2596–2606 (2012).

[5] Bkassiny, M., Li, Y. and Jayaweera, S. K., "A Survey on Machine-Learning Techniques in Cognitive Radios," IEEE Communications Surveys & Tutorials **15**(3), 1136–1159 (2013).

[6] Navarro, P. J., Fernández, C., Borraz, R. and Alonso, D., "A Machine Learning Approach to Pedestrian Detection for Autonomous Vehicles Using High-Definition 3D Range Data," 1, Sensors **17**(1), 18 (2017).

[7] Castaño, F., Beruvides, G., Haber, R. E. and Artuñedo, A., "Obstacle Recognition Based on Machine Learning for On-Chip LiDAR Sensors in a Cyber-Physical System," 9, Sensors **17**(9), 2109 (2017).

[8] Gleason, C. J. and Im, J., "Forest biomass estimation from airborne LiDAR data using machine learning approaches," Remote Sensing of Environment **125**, 80–91 (2012).

[9] Breidenbach, J., Næsset, E., Lien, V., Gobakken, T. and Solberg, S., "Prediction of species specific forest inventory attributes using a nonparametric semi-individual tree crown approach based on fused airborne laser scanning and multispectral data," Remote Sensing of Environment **114**(4), 911–924 (2010).

[10] Weiss, U. and Biber, P., "Plant Detection and Mapping for Agricultural Robots using a 3D-lidar Sensor.," 1 January 2009, 205–210.

[11] Hyyppä, J., Hyyppä, H., Leckie, D., Gougeon, F., Yu, X. and Maltamo, M., "Review of methods of small-footprint airborne laser scanning for extracting forest inventory data in boreal forests," International Journal of Remote Sensing **29**(5), 1339–1366 (2008).

[12] Akay, A. E., Oğuz, H., Karas, I. R. and Aruga, K., "Using LiDAR technology in forestry activities," Environ Monit Assess **151**(1), 117–125 (2009).

[13] Noth, K. R., "Modeling and simulation of a ground based sense and avoid architecture for Unmanned Aircraft System operations," 2011 Integrated Communications, Navigation, and Surveillance Conference Proceedings, O7-1-O7-9 (2011).

[14] Gauci, J. and Zammit-Mangion, D., "Obstacle Detection Around Aircraft on Ramps and Taxiways Through the Use of Computer Vision," AIAA Guidance, Navigation, and Control Conference, American Institute of Aeronautics and Astronautics, Chicago, Illinois (2009).

[15] Behroozpour, B., Sandborn, P. A., Wu, M. C. and Boser, B. E., "Lidar system architectures and circuits," IEEE Communications Magazine **55**(10), 135–142 (2017).

[16] Sandborn, P. A. M., Hariyama, T. and Wu, M.-C., "Resolution-Enhancement for Wide-Range Non-Linear FMCW Lidar using Quasi-Synchronous Resampling," Imaging and Applied Optics 2017 (3D, AIO, COSI, IS, MATH, pcAOP) (2017), paper DW3F.3, DW3F.3, Optica Publishing Group (2017).

[17] Godbaz, J. P., Cree, M. J. and Dorrington, A. A., "Understanding and ameliorating non-linear phase and amplitude responses in amcw lidar," Remote Sensing **4**(1), 21–42 (2012).

[18] Molebny, V., McManamon, P. F., Steinvall, O., Kobayashi, T. and Chen, W., "Laser radar: historical prospective—from the East to the West," OE **56**(3), 031220 (2016).

[19] McManamon, P. F., [LiDAR Technologies and Systems], SPIE Press, Bellingham, WA (2019).

[20] Rairoux, P., Schillinger, H., Niedermeier, S., Rodriguez, M., Ronneberger, F., Sauerbrey, R., Stein, B., Waite, D., Wedekind, C. and Wille, H., "Remote sensing of the atmosphere using ultrashort laser pulses," Applied Physics B **71**(4), 573–580 (2000).

[21] Braun, A., Chien, C., Coe, S. and Mourou, G., "Long range, high resolution laser radar," Optics communications **105**(1–2), 63–66 (1994).

[22] McManamon, P. F., [Field guide to Lidar], SPIE Press (2015).

[23] Bayer, M. M., Torun, R., Li, X., Velazco, J. E. and Boyraz, O., "Simultaneous ranging and velocimetry with multi-tone continuous wave lidar," Opt. Express, OE **28**(12), 17241–17252 (2020).

[24] Swanson, K. J., Jaar, G. S., Mayes, D. C., Mancini, R. C., Ivanov, V. V., Astanovitskiy, A. L., Dmitriev, O., Klemmer, A. W., De La Cruz, C., Dolan, D., Porwitzky, A., Loisel, G. P. and Bailey, J. E., "Development and integration of photonic Doppler velocimetry as a diagnostic for radiation driven experiments on the Z-machine," Review of Scientific Instruments **93**(4), 043502 (2022).

[25] McDonald, J., Pena, M., Satapathy, S., O'Toole, B., Trabia, M. and Jennings, R., "Photon Doppler velocimetry measurements of impact-induced surface waves in glass and their role in fracture initiation and damage evolution," International Journal of Impact Engineering **161**, 104111 (2022).

[26] Levinson, J., Askeland, J., Becker, J., Dolson, J., Held, D., Kammel, S., Kolter, J. Z., Langer, D., Pink, O., Pratt, V., Sokolsky, M., Stanek, G., Stavens, D., Teichman, A., Werling, M. and Thrun, S., "Towards fully autonomous driving: Systems and algorithms," 2011 IEEE Intelligent Vehicles Symposium (IV), 163–168 (2011).

[27] Lukashchuk, A., Riemensberger, J., Karpov, M., Liu, J. and Kippenberg, T. J., "Dual chirped microcomb based parallel ranging at megapixel-line rates," Nat Commun **13**(1), 3280 (2022).

[28] Lihachev, G., Riemensberger, J., Weng, W., Liu, J., Tian, H., Siddharth, A., Snigirev, V., Shadymov, V., Voloshin, A., Wang, R. N., He, J., Bhave, S. A. and Kippenberg, T. J., "Low-noise frequency-agile photonic integrated lasers for coherent ranging," Nat Commun **13**(1), 3522 (2022).

[29] Bayer, M. M., Li, X., Guentchev, G. N., Torun, R., Velazco, J. E. and Boyraz, O., "Single-shot ranging and velocimetry with a CW lidar far beyond the coherence length of the CW laser," Opt. Express, OE **29**(26), 42343–42354 (2021).

[30] Bayer, M. M. and Boyraz, O., "Ranging and velocimetry measurements by phase-based MTCW lidar," Opt. Express **29**(9), 13552–13562 (2021).

[31] Bayer, M. M., Guentchev, G. N., Li, X., Velazco, J. E. and Boyraz, O., "Enhancing the multi-tone continuous-wave lidar with phase detection," 2021, 1182807, International Society for Optics and Photonics.

[32] Peters, R. D., Lay, O. P., Dubovitsky, S., Burger, J. P. and Jeganathan, M., "MSTAR: an absolute metrology sensor with sub-micron accuracy for space-based applications," International Conference on Space Optics — ICSO 2004 **10568**, 709–717, SPIE (2018).

[33] Godbaz, J. P., "Ameliorating Systematic Errors in Full-Field AMCW Lidar," Thesis (2012).

[34] Bhandari, A., et al., "Resolving multipath interference in time-of-flight imaging via modulation frequency diversity and sparse regularization," Opt. Lett., OL **39**(6), 1705–1708 (2014).

[35] Bayer, M. M., Atalar, A., Li, X. and Boyraz, O., "Photonics PNT Based on Multi-Tone Continuous Wave Ranging," Conference on Lasers and Electro-Optics (2022), paper JTh3A.57, JTh3A.57, Optica Publishing Group (2022).

[36] Glorot, X. and Bengio, Y., "Understanding the difficulty of training deep feedforward neural networks."

[37] Kingma, D. P. and Ba, J., "Adam: A Method for Stochastic Optimization," arXiv:1412.6980 (2017).

[38] Sammut, C. and Webb, G. I., "Leave-one-out cross-validation," Encyclopedia of machine learning, 600–601 (2010).